Materials Today Bio 15 (2022) 100292

Contents lists available at ScienceDirect

Materials Today Bio

journal homepage: www.journals.elsevier.com/materials-today-bio

Programmable biological state-switching photoelectric nanosheets for the treatment of infected wounds

Weizhou Ren [a,1], Zefeng Lin [b,c,1], Youzhun Fan [b,1], Jun Xing [b], Guangyu Liu [b], Taizhong Xiao [a], Zhengao Wang [b], Zhengnan Zhou [b], Tao Zhang [c,**], Zhiguo Song [a,***], Peng Yu [b,*], Chengyun Ning [b,d]

[a] School of Materials Science and Engineering, Kunming University of Science and Technology, Kunming, 650093, China
[b] School of Materials Science and Engineering, National Engineering Research Center for Tissue Restoration and Reconstruction, Metallic Materials Surface Functionalization Engineering Research Center of Guangdong, South China University of Technology, Guangzhou, 510641, China
[c] Guangdong Key Lab of Orthopedic Technology and Implant, General Hospital of Southern Theater Command of PLA, The First School of Clinical Medicine, Southern Medical University, Guangzhou, 510515, China
[d] China-Singapore International Joint Research Institute (SSIJRI), Guangzhou, 510000, China

ARTICLE INFO

Keywords:
Bacterial infection
Photoelectric nanosheets
Light-responsive
Antibacterial
Tissue reconstruction

ABSTRACT

Recurrent bacterial infection is a major problem that threatens the tissue repair process. However, most current therapeutic strategies fail to deal with management of the overlap dynamics of bacterial killing and tissue repair. Here, in accord with the different responses of eukaryotic and prokaryotic cells to electric potential, we developed high performance photoelectric BiOCl nanosheets that dynamically switch between conditions that favor either tissue regrowth or antibacterial microenvironments due to light stimulated and bi-modal switching of their surface electrical polarization. *In vitro* assays demonstrate that, under light illumination, the mannitol modified BiOCl nanosheets show high relative surface potential and achieve robust antibacterial performance. Conversely, under dark conditions, the nanosheets exhibit relatively low surface potential and promote Bone Marrow Stem Cell (BMSCs) proliferation. *In vivo* studies indicate that BiOCl nanosheets with light switch capabilities promote the significant regeneration of infected skin wounds. This work offers a new insight into treating recurrent bacterial infections with photoelectric biomaterials for light controlled selection of alternative electrical micro-environments, thereby benefiting the capability for either antisepsis or repair of damaged tissues.

1. Introduction

Bacterial infection is a major obstacle for repair of damaged tissues, ultimately threatening the entire restoration process. Bacterial infections often recur in cases of burns, diabetic abscesses, and chronic diseases [1]. In clinical practice, once damaged tissue is infected, debridement is required to completely remove infected and necrotic tissues. This is usually accompanied by use of a large quantity of antibiotics. However, excessive antibiotic use often induces drug resistance [2,3], and debridement inevitably leads to large amount of scarring [4,5]. Thus, current wound treatment protocols raise critical issues as to how to programmatically eliminate recurrent bacterial infection and promote tissue regeneration.

Recently, a large number of innovative biomaterials activated *via* external stimulation have been developed for modulating cell behavior; these include altering pH, changing electric field polarizations, and activating genes by light exposure. Other materials offer a window of opportunity to improve antibacterial activity or tissue repair by controlling drug release [6–8]. However, they generally focus on promoting either tissue regeneration or antibacterial activity individually, but usually not both. Indeed, it is difficult for the current set of tissue repair materials to integrate both tissue regenerative and antibacterial performance simultaneously, since they are two different biological processes [9–11]. Hence, an intelligent agent that could switch between bioactive

* Corresponding author.
** Corresponding author.
*** Corresponding author.
E-mail addresses: gzlupus@126.com (T. Zhang), songzg@kust.edu.cn (Z. Song), imyup@scut.edu.cn (P. Yu).
[1] These authors contributed equally to this work.

https://doi.org/10.1016/j.mtbio.2022.100292
Received 19 February 2022; Received in revised form 26 April 2022; Accepted 12 May 2022
Available online 16 May 2022

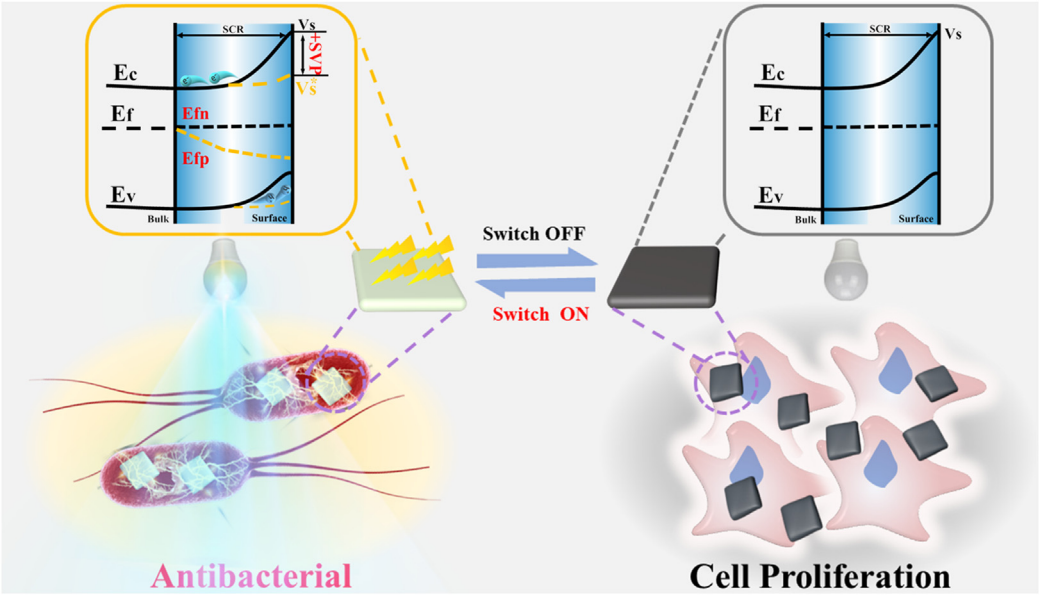

Schematic 1. Schematic diagram of photoelectric BiOCl nanosheets with photoswitch activated selectivity between antibacterial and cell proliferative surface potentials. When light illumination is active, the nanosheets generate a surface photoelectric voltage that enhances its surface potential and affects bacterial cell killing. This state is identified as switch-on. When light illumination is withdrawn, the surface potential returns to a low value and allows cell proliferation. This is identified as the switch-off state. E_C, E_V, E_F, E_{Fn}, E_{Fp}, V_S, V_S* and SPV denote the conduction and valence band edges, the Fermi energy at thermal equilibrium, the quasi Fermi energies of electrons and holes during illumination, the surface potential in the dark, the surface potential under illumination, and the corresponding surface potential, respectively.

ability and antibacterial ability according to the bacterial infection condition would greatly facilitate recurrent bacterial infection treatment.

It is well known that electric polarization plays a central role in many aspects of cellular physiology [12–14]. For example, metabolism and communication among mammalian and bacterial cells are governed *inter alia* by electrical polarization, which involves displacement of large quantities of electrons, protons and charged ions [15]. Polarization of contacting physiological fluids and extracellular matrices present fundamental and useful mechanisms to regulate homeostasis and growth of both mammalian cells and bacteria; it can swing metabolic pathways from their normal paths to acute phase paths. In contrast to bacteria, eukaryotes are known to acquire a fast-inactivation mechanism to electrical potential, making their response to signal patterns different from bacteria [16–18]. A growing number of studies have demonstrated that certain patterns of electrical stimulation produce cell membrane depolarization and certain prescribed ion movements promote cell proliferation [19–21]. It also has been found that high intensity electrical stimulation effectively penetrates bacterial walls and destroys bacteria [22,23]. A controlled electrical potential presents the opportunity to integrate antibacterial activity and cell proliferation programmatically via electrical switching. Many forms of electrical stimulation supplied by external power devices are not suitable for wound healing applications because of their bulkiness and mechanical invasiveness [24]. Thus, we propose that bioactive nanomaterials with strong photoelectric responses may be ideal alternatives, as they are generally not only noninvasive but also capable of producing electrical stimulation using light irradiation as an external stimulus. Although traditional photoelectric materials, like TiO_2, have been used for antibacterial study, their low light absorption properties and low electron-hole separation efficiency limit their practical application [25]. In this work, highly responsive photoelectric BiOCl nanosheets are developed for on-demand photoelectron switching between polarization states to treat infected tissue defect repair.

The right side of Scheme 1 represents the off state for an n-type semiconductive BiOCl. Electrons of the BiOCl nanosheets are captured by surface states and undergo upward band bending that produces a low surface potential. Herein, we demonstrate that this potential promotes mammalian cell proliferation. In the light switch on state (the left part of Scheme 1), photogenerated electrons and holes separate and drift efficiently towards the bulk volume and raise surface electric potential of the BiOCl nanocrystals [26]. Thus, the upward band bending is reduced at the surface, and the surface potential increases with sufficient potential to kill bacteria. We propose a photoelectric device comprising BiOCl nanosheets equipped with an optical window that once injected into an infected wound allows switching surface potentials and alternately promotes mammalian cell proliferation or bacterial killing for healing of wounds in infected tissues.

2. Materials and methods

2.1. Solvothermal synthesis of BiOCl nanosheets

The preparation of BiOCl nanosheets was based on a modified solvothermal method [27]. Typically, 1 mmol Bi $(NO_3)_3 \bullet 5H_2O$ (AR, Aladdin) was dissolved in 60 mL of 0.2 M mannitol solution with 15 min vigorous stirring. Then, NaCl (AR, Aladdin) solution was slowly dropped into the above bismuth source solution with continuous stirring to produce a white suspension. After reacting for 20 min, the solution was transferred into a 100 mL Teflon-lined stainless-steel autoclave to undergo a solvothermal process at 160 °C for 3 h. The product was washed with deionized water and dried at 60 °C.

2.2. Characterization of the BiOCl nanosheets

The phase composition of the obtained products was identified by X-ray diffraction (XRD, Bruker D8-Advance diffractometer) using a diffractometer with Cu Kα irradiation ($\lambda = 1.5406$ nm). The morphology and particle size of the nanosheets were determined by scanning electron microscopy (SEM, Hitachi SU8220) and high-resolution transmission electron microscopy (TEM, JEOL JEM-2100). The UV–vis absorption spectra of the samples were measured on a HITACHI U-4100 spectrophotometer. X-ray photoelectron spectroscopy (XPS, Thermo Escalab 250, Thermo Fisher Scientific, USA) was used for examining the elemental composition of the nanosheets. Containment carbon (C 1s = 284.6 eV) was used to calibrate the binding energy. Fourier transform infrared spectroscopy (FTIR, NICOLET IS10) was used to identify and quantify various chemical groups on the nanosheets. An ultraviolet–visible–near-infrared spectrophotometer (UV-3600, Shimadzu, Japan) was used for the absorbance measurements of various samples.

2.3. Photoelectric characterization of the BiOCl nanosheets

Kelvin probe force microscopy (KPFM) measurement was carried out using an Asylum Research MFP-3DTM atomic force microscope in non-contact mode. The cantilever was coated with a Pt Ir alloy and used for

KPFM modes. The BiOCl nanosheet samples were tested in a dark environment and under the excitation of 365 nm LED lights. The surface photovoltaic spectroscopic (SPV) measurement was carried out using chopped light and a lock-in amplifier to remove DC noise. The lock-in amplifier (SR830-DSP) and light chopper (SR540) provided signal encoding. All the measurements were performed at room temperature. Photocurrent measurements on the BiOCl nanosheets was tested with switching between on/off cycles using a standard three-electrode system and the Na_2SO_4 (0.5 mol L^{-1}) solution as the electrolyte [28]. An electrochemical workstation provided the programming for electrode voltages and current detection. A 365 nm LED was utilized as light source.

2.4. In vitro antibacterial activity assay of BiOCl nanosheets in the switch on/off states

Single colony colonies of *E. coli* (ATCC 25922) and *S. aureus* (ATCC 25923) bacteria were collected from Luria−Bertani (LB) agar plates and transferred to 10 mL of LB broth, respectively. After 10 h culture at 37 °C, the bacteria in LB broth were centrifuged to isolate single strains and then suspended in PBS solution for measuring the optical turbidity at 600 nm with microplate reader. To investigate the antibacterial action under light switching, 250 mg mL^{-1} BiOCl nanosheet samples were cultured with *E. coli* or *S. aureus* bacteria at a concentration of 1.0×10^6 CFU mL^{-1}. For the light illuminated samples, BiOCl nanosheets and blank control were cultured with bacteria under 365 nm LED illumination for 30 min. For the light off groups, BiOCl nanosheets and blank control were cultured with bacteria in the dark. Bacteria were then diluted 100-fold in PBS solution. Subsequently, 50 μL of the dilution was spread on LB agar plates and incubated at 37 °C. To determine the antibacterial efficacies of BiOCl nanosheets against *E. coli* and *S. aureus*, *E. coli* and *S. aureus* cultures were repeatedly mixed with BiOCl nanosheets and illuminated under LED light for 30 min up to four times. No additional sterilization was employed during the procedure. The bacterial killing ratio was calculated as follows in Equation (1):

$$Bacterial\ \ Killing\ \ ratio(\%) = \frac{CFU_{(Blank)} - CFU_{(sample)}}{CFU_{(Blank)}} * 100\% \quad (1)$$

2.5. Observation of bacterial morphology

After the bacteria suspension was treated according to the above procedures, the bacteria were fixed with 2.5% glutaraldehyde for 4 h, rinsed with PBS 3 times, and dehydrated with series ethanol solutions (30, 50, 70, 90, and 100 v/v%) successively for 15 min each, and then transferred to isoamyl acetate for 20 min, and finally dried in air. Finally, the bacterial samples were inspected by SEM (Zeiss EVO18, Carl Zeiss Company, Germany).

2.6. Live/dead bacterial viability assay

Live/dead fluorescent staining of bacteria were used to characterize the viability of bacterial. After being co-cultured with the BiOCl nanosheets under irradiation of 365 nm with a LED source for 30 min, the bacterial were stained with the LIVE/DEAD Bac-Light bacterial viability kit and photographed with an Inverted fluorescence microscope (Zeiss, Axio Observer, Germany); dead bacteria fluoresce in red while live bacteria fluoresce in green.

2.7. Measurement of reactive oxygen species (ROS) generation

A ROS-sensitive probe, dichloride-fluorescein diacetate (DCFH-DA), which is an oxidation-sensitive fluorescent dye, was used to detect ROS generation of treated bacteria. In brief, 250 mg mL^{-1} BiOCl co-cultured with bacteria were immersed in the above fluorescent dye solution and exposed to light irradiation for 30 min. The intracellular ROS levels were recorded through the fluorescence change in the solution with an excitation wavelength of 488 nm and an emission wavelength of 525 nm.

2.8. Cell proliferation assay

To evaluate cell proliferation on BiOCl nanosheets, bone marrow mesenchymal stem cells (BMSCs, CRL-12424, ATCC, USA) were cultured with BiOCl and analyzed using the Cell Counting Kit-8 (CCK-8). Briefly, BMSCs were seeded in 96-well cell culture plates at densities of 2500 cell per well in DMEM containing 10% FBS at 37 °C in a humid atmosphere of 5% CO_2. After 24 h incubation, the cells were incubated with BiOCl nanosheets of different concentrations. Cells, cultured in the medium without nanomaterials, were used as the negative control. After an additional 24 h of incubation, 10 μL of the CCK-8 reagent (Dojindo, Japan) was added, and the culture was incubated another 2 h at 37 °C. The optical density was measured using a spectral scanning multimode reader (Thermo Scientific Varioskan Flash, USA) at a 450 nm wavelength. For light illuminated groups, cells were cultured with nanosheets in the same manner as the aforementioned process. After cells were incubated with BiOCl nanosheets for 24 h, the nanosheets and blank controls were illuminated at 365 nm with a LED source at a power density of 4.25 mW cm^{-2} for 30 min, then the same condition with normal CCK-8 tests.

2.9. Live/dead cell staining assays

To further confirm that BiOCl nanosheets are biocompatible with BMSC cell viability, the cells were stained with the calcein-AM (green for living cells)/propidium iodide (PI, red for dead cells) and examined microscopically. The cells were stained for 30 min at room temperature and subsequently washed with PBS, and finally observed with an inverted fluorescence microscope (Nikon Eclipse Ti–U, Japan).

2.10. Membrane potential assays

Cell membrane potential was measured using the fluorescence dye DiBAC4(3) (Dojindo, Japan). BMSCs were seeded on a confocal dish at a density of 4×10^4 cells/well. After culturing for 24 h, the cells were washed with DPBS, and then incubated with 5 μmol/L DiBAC4(3) diluted with 20 mmol/L 4-(2-hydroxyethyl)-1-piperazineethanesulfonic acid (HEPES, Sigma Aldrich, USA) for 30 min at 37 °C, in the dark. Subsequently, A photograph was taken as the initial state, followed by the addition of BiOCl nanosheets and PBS, and then photographed at 1 min intervals as the final state. Fluorescence images of the cells were examined by a confocal laser scanning microscope and analyzed using Image J software.

2.11. Scratch wound assay

BMSCs were seeded in 6-well plates (2×10^5 cells/well) overnight. Once cells were confluent, the layer was scratched with a 20 μL pipette tip and was washed three times with Dulbecco's phosphate buffered saline (DPBS, Gibco, USA). The 250 mg mL^{-1} BiOCl nanosheet and media without material was then added and treated under light off and light illumination (365 nm LED) for 30 min. Images were captured with an inverted fluorescence microscope at 0 and 24 h; then, the cell migration rate was analyzed with Image J software.

2.12. In vivo infected skin wound regeneration

All animal experiments and procedures were approved by the General Hospital of Southern Theater Command. All animals were kept and utilized in accordance with the Animal Management Rules of the Ministry of Health of the People's Republic of China and the Guidelines for the Care and Use of Laboratory Animals of China. In brief, 12-week-old female SD rats were used to model infected surface wounds. Two round, full-thickness skin wounds (~φ10 mm) were created by excising dorsal

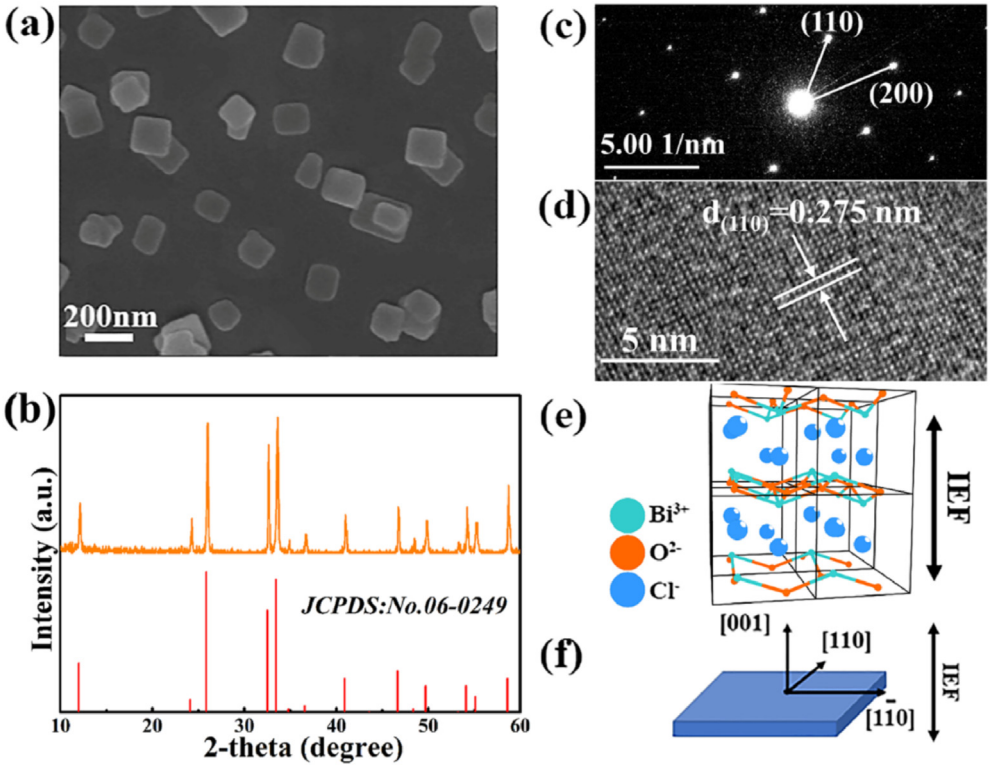

Fig. 1. Characterization of the BiOCl nanosheets. (a) and (b) SEM image and XRD patterns of BiOCl nanosheets. (c) SAED pattern, and (d) HRTEM image of the BiOCl nanosheets. (e) Atomic structure of the BiOCl nanosheets. (f) Schematic illustration of crystal structure and orientation of the BiOCl nanosheets. The results indicate that the BiOCl nanosheets with {110}facets exposed were successfully prepared.

skin sections with using a biopsy puncher. The wounds were infected by infusing 50 μL (10^6 CFU mL^{-1}) of *S. aureus* for 1 h. Then SD rats with infected wounds were randomly divided into 3 groups. Group I: 50 μL suspension of BiOCl nanosheets at a concentration of 250 μg/mL was applied dropwise to the skin wound and treated with light (365 nm LED) for 30 min, then returned to dark conditions. Group II: 50 μL suspension of BiOCl nanosheets at a concentration of 250 μg/mL was applied dropwise to the skin wound and under dark conditions for duration of the experiment. Group III: 50 μL PBS solution was applied dropwise to the skin wound and treated with light (365 nm LED) for 30 min, and then returned to dark conditions. The animals were individually housed in cages and allowed to heal for 14 days. At days 3, 7, 10 and 14, the areas of the wounds were measured and photographed. At days 7 and 14, the skin tissue samples were excised and fixed with 10% formalin for pathological slides. At the termination of the experiments, the animals were sacrificed. Samples of granulation tissue were removed from formaldehyde solution, dehydrated, and then embedded in paraffin. Hematoxylin and eosin (H&E) staining and Masson's trichrome staining were used for cell identification. A microtome was used to prepare serial sections in accordance with standard protocols. After staining, the histological sections were imaged and recorded by 3DHISTECH Case Center.

2.13. Statistical analysis

All data are presented as the mean ± standard deviation. Significant differences were determined using a one-way analysis of variance (ANOVA) and Student's test in SPSS 17 (IBM, Armonk, New York, USA) software ($n = 4$), "**" $p < 0.01$ and "*" $p < 0.05$ are statistically significant.

3. Results and discussion

3.1. Fabrication and characterization of BiOCl nanosheets with optical switch properties

BiOCl nanosheets were prepared by one-step solvothermal synthesis, using bioactive mannitol as both a capping agent and modifier [29]. The prepared samples show square-like nanosheet structures with widths of ~150 nm (Fig. 1a). And Energy Dispersive Spectrum (EDS) shows the nanosheets is composed of Bi, Cl, O element (Fig. S1). The X-ray diffraction (XRD) pattern also proves that diffraction peaks of the nanosheets are consistent with the tetragonal BiOCl (JCPDS No. 06–0249) (Fig. 1b), which confirms the BiOCl nanosheets are successfully prepared. Furthermore, the adjacent angle marked in the selected-area electron diffraction (SAED) pattern is 45°, which is consistent with the theoretical angle between the (110) and (200) crystal planes. And the lattice fringe spacing is 0.275 nm, corresponding to the (110) crystal plane, indicating that the BiOCl nanosheets possess highly exposed {110} facets (Fig. 1c and d). The elemental composition and surface chemical state of the BiOCl nanosheets were further analyzed using XPS spectroscopy (Fig. S2a-S2b). The survey spectrum of the BiOCl nanosheets indicating the existence of three elements Bi, O, and Cl. From the high-resolution XPS spectrum, the presence of polyhydroxy groups on the surface indicated that mannitol molecules were incorporated into the BiOCl crystals and guided its growth. Meanwhile, FI-IR spectroscopy was used to demonstrate the modification of BiOCl crystals by mannitol molecules (Fig. S2c). Due to the polarization caused by its unique layered crystalline structure, the spontaneous internal electric fields (IEF) form along the [001] direction. This configuration gives rise to the existence of the driving force potential for photocharge separation (Fig. 1e) [26].

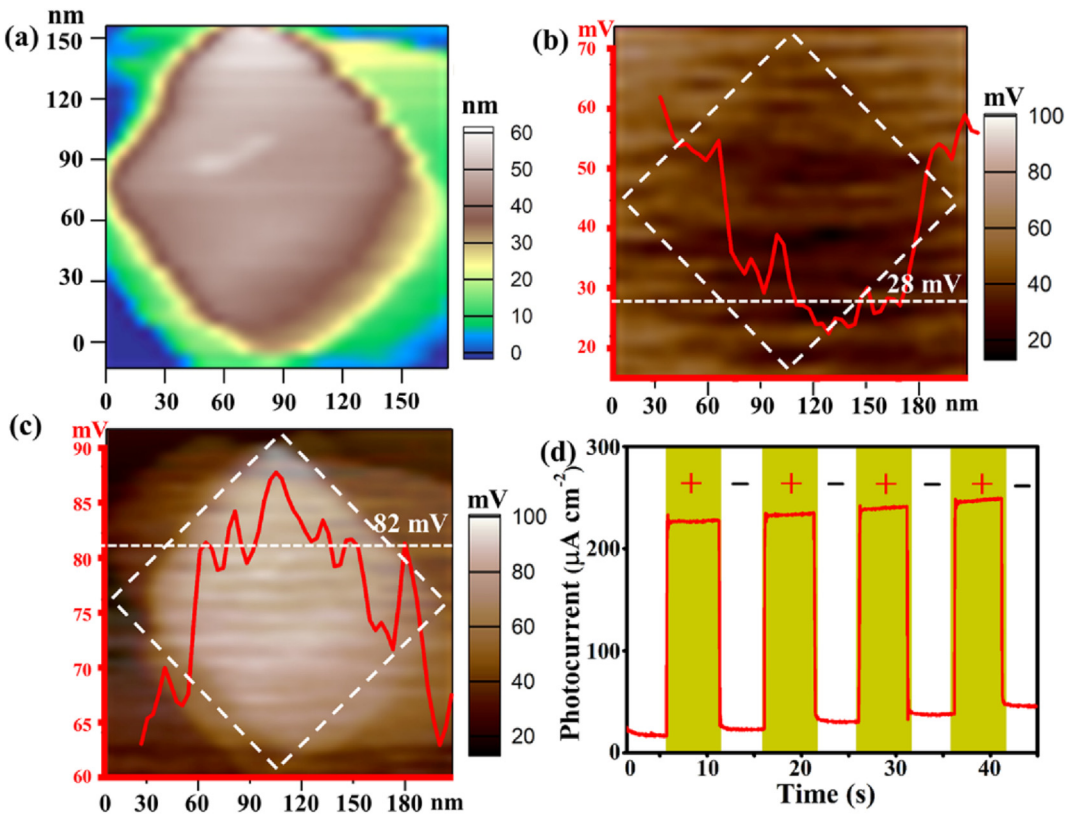

Fig. 2. AFM Characterization of photoelectric switching in BiOCl nanosheets. (a) AFM characterization of the surface topography of nanosheets. (b) and (c) KPFM characterization of the surface potential of BiOCl nanosheets under changes of state of the light switch: (b) off state, (c) on state. The results show that the BiOCl nanosheet under illumination (on state) is ~54 mV higher than under no illumination (off state). (d) Photocurrent responses of the BiOCl nanosheets with cycling the illumination source (positive sign for switch on; negative sign for switch off). The results indicate that BiOCl nanosheets possess reversible photoelectric performance.

Therefore, when the BiOCl nanosheets present the dominant exposure of {110}facets (Fig. 1f), the combination oriented IEF and the small thickness of the nanosheets make it possible for photogenerated holes to drift to the surface. These features enable the increase in the surface potential of the nanosheets to kill the bacteria.

To evaluate the photoelectric response, the surface potential change under light illumination was detected by Kelvin Probe Force Microscopy (KPFM) [30]. Atomic Force Microscopy images reveal that the prepared BiOCl comprise smooth, square-like nanosheets (Fig. 2a). Fig. 2b and c shows that under light illumination, the relative local surface potential of the sample increases from ~28 to ~82 mV.

To further evaluate their photoelectric response, we measured the surface photovoltaic voltage spectra (SPV) of the prepared BiOCl nanosheets (Fig. S3). The SPV curve is consistent with the reported band gap of BiOCl semiconductors, showing the typical broad response band from 280 to 410 nm. These findings indicate that under inter-band excitation, the photoinduced holes separate and transfer to surface, leading to a sharp increase in surface potential. Additionally, to further confirm the photosensitive response and the reversibility of the switching effect, transient photocurrents were measured with periodic light illumination. The results show that the BiOCl nanosheets generate a steady-state photocurrent of 200 nA cm^{-2} under light illumination, showing a rapid and reversible photoresponse that follows the light switch cycles. This indicates that the prepared BiOCl nanosheets have highly sensitive and reversible light-activated surface potentials.

3.2. Light activated, antibacterial assay in vitro

To characterize the effectiveness of the light switchable antibacterial property of the BiOCl photoelectric nanosheets, we carried out plate counting assays. After culture in the light off state, we found no remarkable change in the number of *E. coli* and *S. aureus* colonies (Fig. 3). Culture in the light on state, however, produced significantly enhanced bactericidal efficiency. In the light on state, BiOCl photoelectric nanosheets kill almost all the bacteria, with antibacterial ratios of 99.24% and 99.54% on *E. coli* and *S. aureus*, respectively (Fig. 3b and (e)). After that, the BiOCl photoelectric nanosheets were harvested for the next cycle of antibacterial test. The photoelectric antibacterial tests of BiOCl were carried out over four cycles in the light on/off state, with an over 96% and 95% antibacterial ratio for *E. coli* and *S. aureus*, respectively, thus demonstrating that the nanosheets exhibit reversible antibacterial performance (Fig. S4).

External electric field might enhance plasma membrane permeabilization, and cause reactive oxygen species production by affecting the respiratory process to cause cell death [31,32]. To explore the light switchable antibacterial mechanism of BiOCl nanosheets, the intracellular reactive oxygen species (ROS) levels were measured under the light switch off/on state. As shown in Fig. 3c and f, under the light on state, the ROS levels of both *E. coli* and *S. aureus* bacteria were significantly increased compared to the blank control. The fluorescent images (Fig. S5) show that the BiOCl nanosheets haved the largest number of dead *E. coli* and *S. aureus* cells with the light on state, showing strong antibacterial abilities. These results are consistent with the results of the plate count results analysis. The morphologies of bacteria (*E. coli* and *S. aureus*) interacting with BiOCl nanosheets were qualitatively evaluated by SEM images. As shown in Fig. 3g and h, in the presence of the BiOCl nanosheets in the light off state, the morphology of *E. coli* and *S. aureus* exhibits pronounced edges and intact cell walls. After 30 min in the light on state, both *E. coli* and *S. aureus* adhere to the nanosheets where the cell walls become rough, wrinkled, or riddled with cracks. According to the above results, high surface potential of photoelectric BiOCl in the light on state inhibits the activity of proteins and the metabolism of bacteria

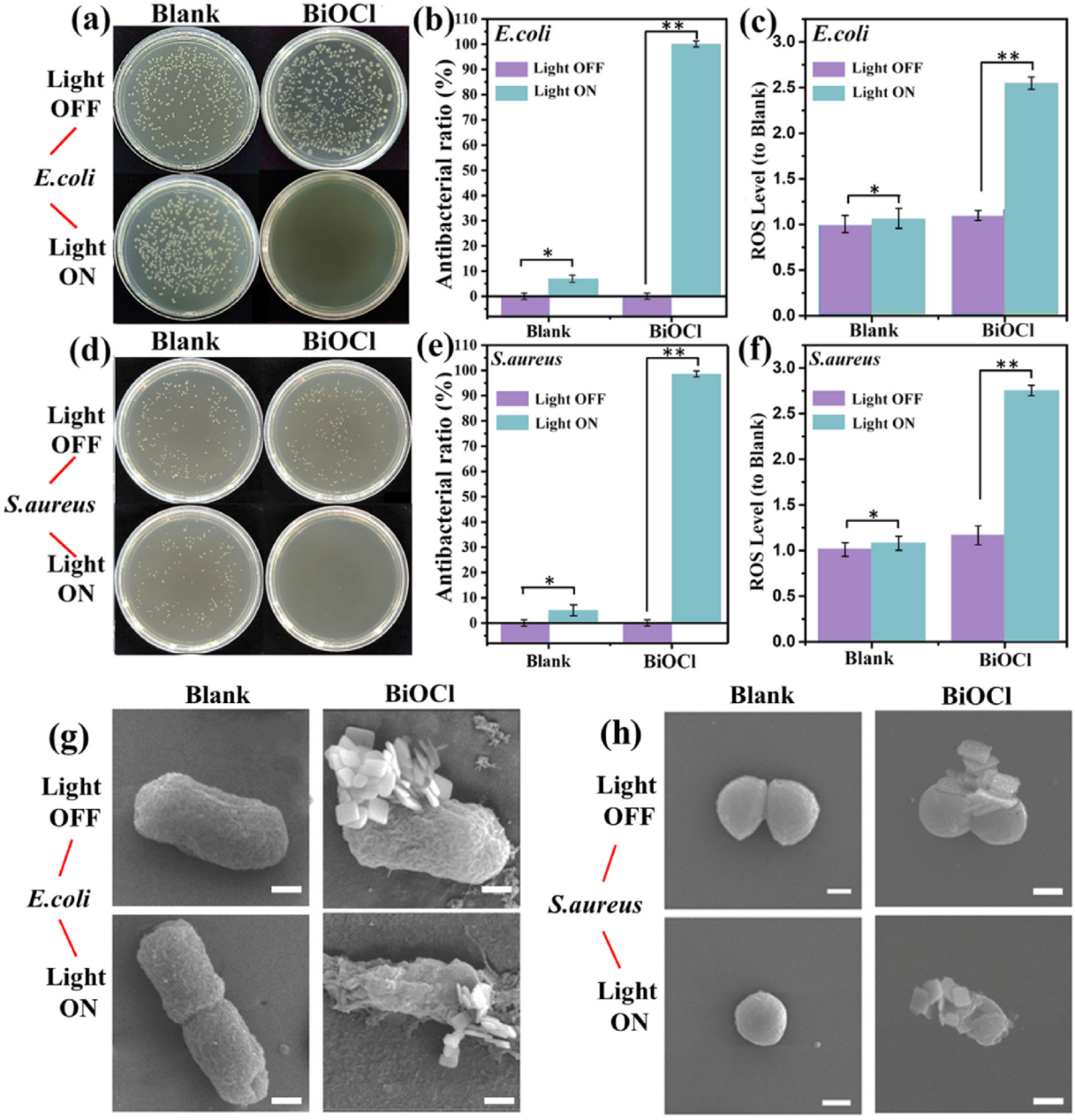

Fig. 3. *In vitro* antibacterial assay of BiOCl photoelectric nanosheets under light switch off/on states. Plate counting assay of (a) *E. coli*. and (d) *S. aureus* cultured in the presence of BiOCl. The corresponding antibacterial ratio of the nanosheets from the surviving colony fractions of *E. coli* (b) and from *S. aureus* (e) under one of the bimodal conditions of light activation. The ROS levels in *E. coli* (c) and *S. aureus* (f) were analyzed by DCFH-DA probe assay by switching the bimodal light trigger. Fluorescent intensity was normalized by initial fluorescent intensity of the Blank (F_L/F_{L0}). (g–h) Representative SEM images of bacteria treated with BiOCl nanosheets under light switch off and on states. The scale bar is 200 nm. The experiment was performed in independent triplicates. Data is presented as mean ± SD (*P < 0.05, **P < 0.01, ***P < 0.001). The results indicate that the killing of bacteria by nanosheets can be switched on and off under light activation.

while the nanosheets produce intracellular ROS species that lead to oxidative stress and damaged membranes and finally causes the destruction of bacterial membrane and the death of bacteria [33].

3.3. *In vitro* mammalian cell culture in presence of BiOCl photoelectric nanosheets under light off/on states

The live/dead staining assay was carried out to examine the toxicity of BiOCl nanosheets on BMSCs. As shown in Fig. 4a, no dead cells were observed under either the light switch off/on states. These results indicate that BiOCl nanosheets in culture with BMSC cells have good biocompatibility. CCK-8 assay was performed to quantify BMSCs proliferation in the presence of BiOCl photoelectric nanosheets under light and no light conditions. As shown in Fig. 4b, in the light off state, the cell proliferation ratio increased about 19% compared to the blank control group. In the light on state, the cell proliferation ratio decreased by about 5% compared to the blank control group. The test showed this occurred without a statistical difference. The cell viability was over 98% even at a concentration as high as 500 μg mL^{-1} in the absence of light irradiation, presenting a viability of 98% at the light on state at the same time (Fig. S6). These results demonstrate that BiOCl photoelectric nanosheets promote BMSC cell proliferation in the light off state, and do not influence cell viability in the light on state.

We further compared the cell membrane potential of BMSCs cultured with BiOCl photoelectric nanosheets and blank control using DiBAC4(3). The results indicate that the cell membrane potential of cells cultured on

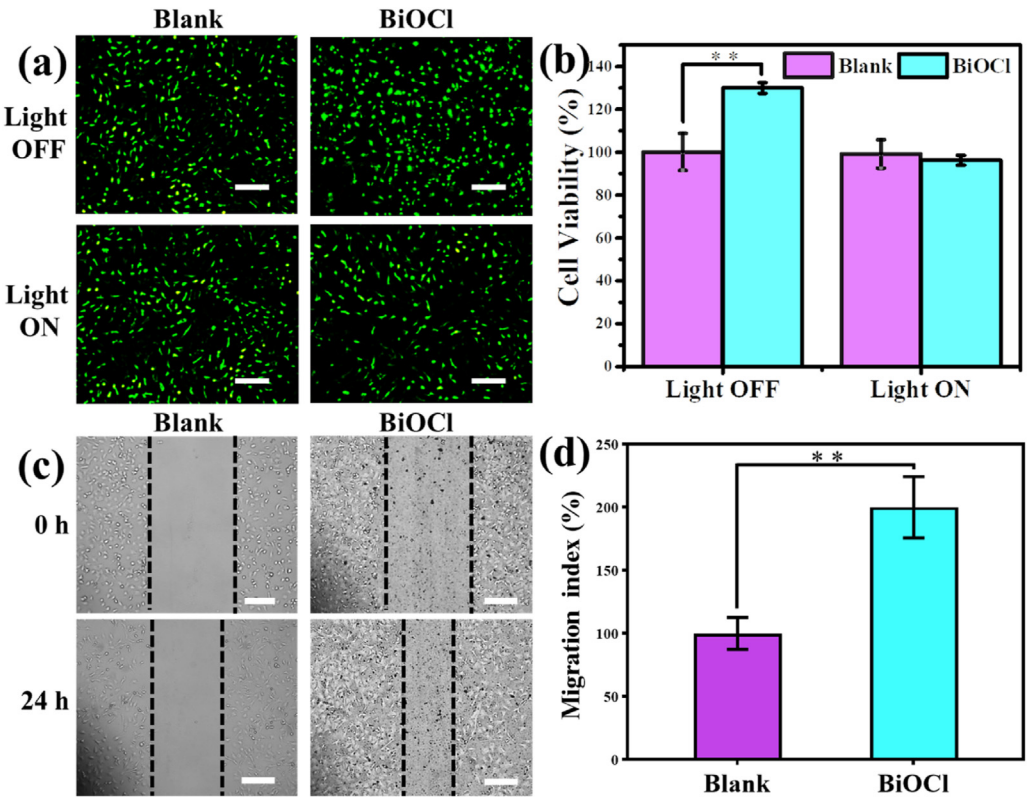

Fig. 4. *In vitro* assessment of BiOCl nanosheet biotoxicity and cell proliferation. (a) Fluorescence images of live/dead BMSCs grown on the BiOCl photoelectric nanosheets. The scale bar = 20 μm. BMSCs were stained with Calcein AM for live cells (green) and Propidium Iodide (PI) for dead cells (red). (b) Cell viability of BMSCs as measured using the CCK-8 method. (c) Representative migration images and (d) migration index statistics of BMSCs after co-culture on the BiOCl photoelectric nanosheets at 0 and 24 h. The scale bar = 200 μm. The experiments were performed in independent triplicate (*P < 0.05, **P < 0.01, ***P < 0.001). The results demonstrate that the BiOCl nanosheets are bioactive under light switch control, and promote BMSCs proliferation in the light off state.

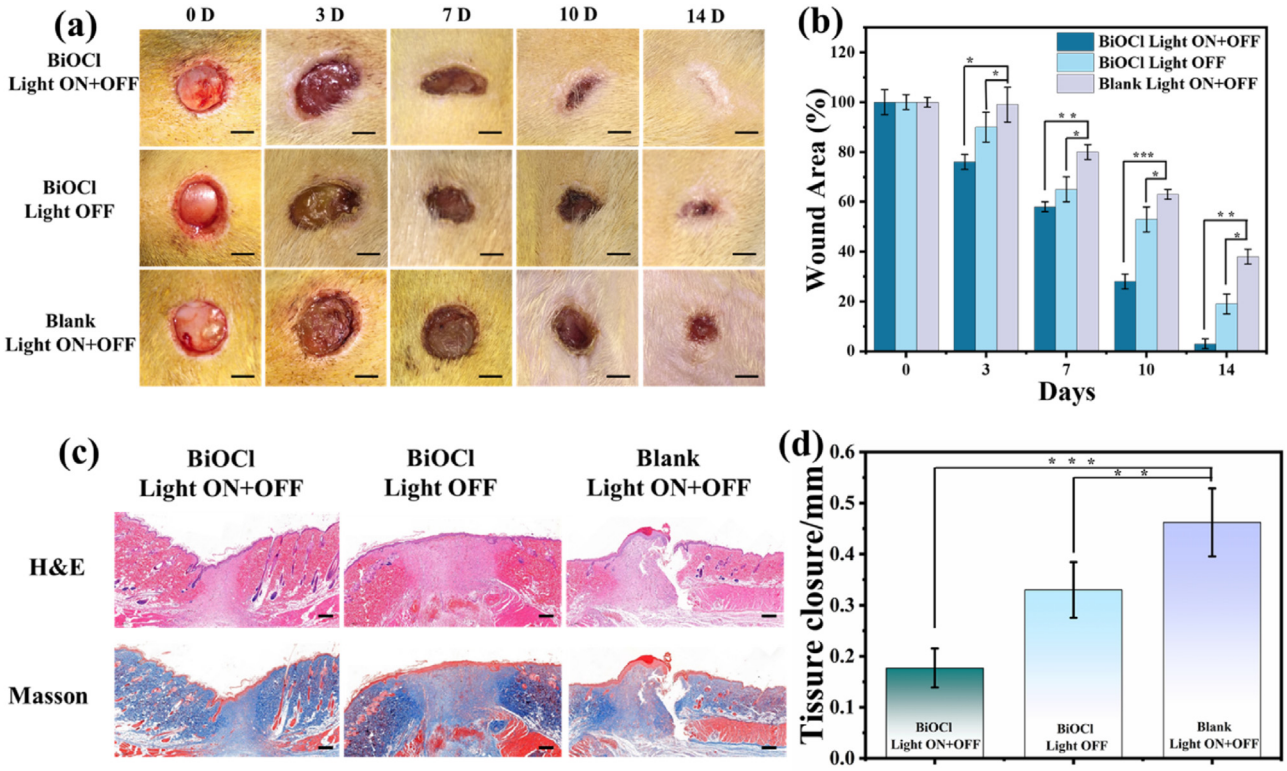

Fig. 5. *In vivo* evaluation of healing rate of infected skin wounds by BiOCl nanosheets. (a) Low magnification micrographs (scale bars, 5 mm) and (b) statistical summary of wound closure rates of the infected wounds *in vivo* when treated with BiOCl photoelectric nanosheets and controls. Data were obtained at time points of 0, 3, 7, 10, and 14 days after wound opening. (c) H&E and Masson staining images of the infected wounds treated with nanosheets and controls under different light states after 14 days. Scale bars are 500 μm. (d) Quantitative analysis of tissue closure in each group after 14 days of treatment. Data is reported as mean ± SD (*P < 0.05, **P < 0.01, ***P < 0.001).

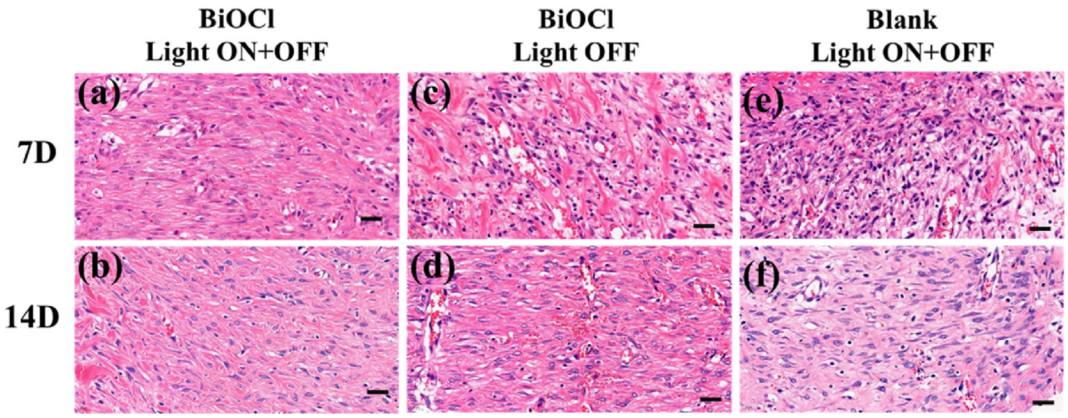

Fig. 6. *In vivo* evaluation of the state of inflammation tissues at the infected wound site. Highly magnified image of hematoxylin and eosin (H&E) histological staining at the infected wound site at 7 and 14 days with and without light triggered nanosheet therapy. Nanosheet and control samples are identified. Scale bar is 20 μm.

BiOCl photoelectric nanosheet was lower than that of cells cultured on blank group under the light switch off state (Fig. S7), reaching a cell depolarization state. This is consistent with previous researches that cells tend to proliferate under depolarization state. In addition, the ability of cells to migration is a key factor in tissue healing and further scratch experiments were performed to assess the effect of BiOCl nanosheets on cell migration (Fig. 4c and d). After scratch treatment and co-culture for 24 h, the scratch healing of BMSCs cells in the blank group was slow, while the scratch area of cells in the BiOCl nanosheets group was significantly reduced. In conclusion, the photoelectric nanosheets could promote cell migration and facilitate tissue repair.

3.4. *In vivo animal experiments*

The effect of light-switchable photoelectric nanosheets on infected wound healing was evaluated in a rat skin wound model. Skin wounds with a diameter of 10 mm were created on the dorsal skin of the rat, and then infected with *S. aureus*. The wound lesions were treated by imposing one of three conditions in three different groups. BiOCl nanosheets were present with the wound irradiated for 30 min and then transitioned to the light off state. In a second group, BiOCl nanosheets were present and maintained continuously in the light off state. Finally, as a negative control, a third group having no nanosheets present in the wound were given illumination for 30 min, and then the wound illumination was switched off for the duration of the experiment.

As shown in Fig. 5a, the skin wound showed significant regeneration at day 3 in the group treated with BiOCl nanosheets with 30 min illumination. However, the skin wound was still suppurative in the group treated with BiOCl nanosheets without illumination. In the negative control group that received 30 min illumination, the skin wound was suppurative at day 3, which was attributed to the presence of bacteria. After 7 days, wound closure of the group treated with BiOCl nanosheets under light was more noticeable compared to other groups. After 14 days, the group treated with BiOCl nanosheets under light had almost healed, while the no light and the sans nanosheet control groups displayed wound eschars. Further quantification confirms that nanosheets with light accelerates wound closure and reduces scar formation. We attribute this to the destruction of bacteria by the photoelectric effect and the promotion of cell proliferation and tissue regeneration by the BiOCl (Fig. 5b).

Hematoxylin and eosin (H&E) and Masson histological stains were used to further assess the tissue regeneration at the wound site. As shown in Fig. 5c, the H&E staining images show the more mature follicles grow in the BiOCl nanosheets with light on/off switch group than in the control. Masson's staining of regenerated tissue also demonstrates that BiOCl nanosheets produce the most newly formed collagen in the dermal layer. In addition, highly magnified, H&E stained images of regenerated tissues were used to histologically analyze wound recovery. As shown in Fig. 6, the inflammatory response caused by the invading bacteria was severe. Immune cells occupied large areas at the defect site after 7 days for the samples where nanosheets were not illuminated (Fig. 6c). Hardly any inflammatory cells can be observed in the 7 days samples containing nanosheets that were illuminated (Fig. 6a). The growth of bacteria was thus inhibited by elevated surface potentials. The reduction of inflammation at the early stage suggests a role in reducing bacterial populations.

The enhanced regeneration of the wounded skin tissue can be attributed to the ability of BiOCl nanosheets with light-induced surface potential regulation, which can rationally switch between antibacterial priority and proliferation priority. When the photoelectric nanosheets adhere to the wound surface, they dynamically reconstruct bacterial and bioactive electro-microenvironments [34,35], which promotes enhanced wound healing. In the past few years, various antibacterial agents, such as ion incorporated nanoparticles, photothermal/photodynamic graphene and antibacterial polymers [36–38], have been developed for fighting tissue infection. However, coordinated control of antibacterial action and tissue regrowth remains a challenge. In comparison, the photoelectric BiOCl nanosheets with photo-active switching between antibacterial action and mammalian cell activation provide a non-invasive and non-genetic means to programmatically eliminate recurrent bacterial infection and promote tissue regeneration. In the future, the BiOCl nanosheets can be recombined with photosensitizers to extend the light absorption to the near-infrared regime, which will extend the BiOCl nanosheet use to deep inner tissues.

4. Conclusion

In this study, we synthesized bioactive BiOCl photoelectric nanosheets and demonstrated that they achieve switchable bioactivity that alternates between antibacterial action and stimulation of tissue regrowth, depending on the state of light illumination. The nanosheets possess fast light induced surface potential changes of greater than 50 mV between light on/off states. In the switch on state, 98.60% *E. coli* and 99.0% *S. aureus* are killed within 30 min of light exposure. This is attributed to the rapid and elevated positive surface potential. In the light off state, the nanosheets exhibit a lower surface potential that facilitates endogenous cell proliferation. In vivo experiments further demonstrate that BiOCl photoelectric nanosheets with switching options promote skin wound reconstruction. In summary, this research utilizes the photoswitch aspect of a new material to change its surface potential to develop an application for the therapeutic intervention into recurrent tissue infections. We expect this to apply broadly in the treatment of various human tissue infections.

Author contributions

W.R., Z.L., and Y.F. designed and performed the experiments. P.Y., W.R. drafted the manuscript. W.R. constructed samples. G.L., J.X. and Z.Z. and participated in data analysis. T.X. and W.R. performed the surface characterization. P.Y., Z.S. and T.Z. initiated the design of the study and revised the manuscript. C.N., and Z.W. supervised the study and revised.

Data availability

The data that support the findings of this study are available from the corresponding author upon reasonable request.

Credit author statement

W.R., Z.L., and Y.F. designed and performed the experiments. P.Y., W.R. drafted the manuscript. W.R. constructed samples. G.L., J.X. and Z.Z. and participated in data analysis. T.X. and W.R. performed the surface characterization. P.Y., Z.S. and T.Z. initiated the design of the study and revised the manuscript. C.N., and Z.W. supervised the study and revised.

Declaration of competing interest

The authors declare that they have no known competing financial interests or personal relationships that could have appeared to influence the work reported in this paper.

Acknowledgements

This work is supported by National Natural Science Foundation of China (Nos. 11874186, 52072127, 51932002, 52003085), Science and Technology Program of Guangzhou (No. 202002030308), Foundation of China-Singapore International Joint Research Institute (No. 203-A018004), the China Postdoctoral Science Foundation (No. 2020M672642), the Natural Science Foundation of Guangdong Province (2018A030313073). Prof. Tao Zhang works on this fundation.

Appendix A. Supplementary data

Supplementary data to this article can be found online at https://doi.org/10.1016/j.mtbio.2022.100292.

References

[1] D. Han, Y. Li, X. Liu, B. Li, Y. Han, Y. Zheng, K.W.K. Yeung, C. Li, Z. Cui, Y. Liang, Z. Li, S. Zhu, X. Wang, S. Wu, Rapid bacteria trapping and killing of metal-organic frameworks strengthened photo-responsive hydrogel for rapid tissue repair of bacterial infected wounds, Chem. Eng. J. 396 (2020) 125194.
[2] J.M.V. Makabenta, A. Nabawy, C.-H. Li, S. Schmidt-Malan, R. Patel, V.M. Rotello, Nanomaterial-based therapeutics for antibiotic-resistant bacterial infections, Nat. Rev. Microbiol. 19 (1) (2021) 23–36.
[3] X. Zhang, Z. Zhang, Q. Shu, C. Xu, Q. Zheng, Z. Guo, C. Wang, Z. Hao, X. Liu, G. Wang, W. Yan, H. Chen, C. Lu, Copper clusters: an effective antibacterial for eradicating multidrug-resistant bacterial infection in vitro and in vivo, Adv. Funct. Mater. 31 (14) (2021) 2008720.
[4] J. Li, X. Liu, L. Tan, Z. Cui, X. Yang, Y. Liang, Z. Li, S. Zhu, Y. Zheng, K.W.K. Yeung, X. Wang, S. Wu, Zinc-doped Prussian blue enhances photothermal clearance of Staphylococcus aureus and promotes tissue repair in infected wounds, Nat. Commun. 10 (1) (2019) 4490.
[5] Y. Ren, H. Liu, X. Liu, Y. Zheng, Z. Li, C. Li, K.W.K. Yeung, S. Zhu, Y. Liang, Z. Cui, S. Wu, Photoresponsive materials for antibacterial applications, Cell Rep. Phys. Sci. 1 (11) (2020) 100245.
[6] F. Nazir, T.A. Tabish, F. Tariq, S. Iftikhar, R. Wasim, G. Shahnaz, Stimuli-sensitive Drug Delivery Systems for Site-specific Antibiotic Release, Drug Discovery Today, 2022.
[7] M. Aflori, Smart nanomaterials for biomedical applications-A review, Nanomaterials 11.2 (2021) 396.
[8] J. Xu, X. Zhou, Z. Gao, Y.-Y. Song, P. Schmuki, Visible-light-triggered drug release from TiO_2 nanotube Arrays: a controllable antibacterial platform, Angew. Chem. Int. Ed. 55 (2) (2016) 593–597.
[9] A. Kushwaha, L. Goswami, B.S. Kim, Nanomaterial-based therapy for wound healing, Nanomaterials 12 (4) (2022) 618.
[10] J. Xu, Y. Li, H. Wang, M. Zhu, W. Feng, G. Liang, Enhanced antibacterial and anti-biofilm activities of antimicrobial peptides modified silver nanoparticles, Int. J. Nanomed. 16 (2021) 4831–4846.
[11] X. Zhao, B. Guo, H. Wu, Y. Liang, P.X. Ma, Injectable antibacterial conductive nanocomposite cryogels with rapid shape recovery for noncompressible hemorrhage and wound healing, Nat. Commun. 9 (1) (2018) 2784.
[12] X. Dai, B.C. Heng, Y. Bai, F. You, X. Sun, Y. Li, Z. Tang, M. Xu, X. Zhang, X. Deng, Restoration of electrical microenvironment enhances bone regeneration under diabetic conditions by modulating macrophage polarization, Bioact. Mater. 6 (7) (2021) 2029–2038.
[13] M. Zhao, B. Song, J. Pu, T. Wada, B. Reid, G. Tai, F. Wang, A. Guo, P. Walczysko, Y. Gu, T. Sasaki, A. Suzuki, J.V. Forrester, H.R. Bourne, P.N. Devreotes, C.D. McCaig, J.M. Penninger, Electrical signals control wound healing through phosphatidylinositol-3-OH kinase-γ and PTEN, Nature 442 (7101) (2006) 457–460.
[14] Z. Schofield, G.N. Meloni, P. Tran, C. Zerfass, G. Sena, Y. Hayashi, M. Grant, S.A. Contera, S.D. Minteer, M. Kim, A. Prindle, P. Rocha, M.B.A. Djamgoz, T. Pilizota, P.R. Unwin, M. Asally, O.S. Soyer, Bioelectrical understanding and engineering of cell biology, J. R. Soc. Interface 17 (166) (2020) 20200013.
[15] P. Yu, G. Tan, X. Deng, Z. Wang, C. Ning, L. Ding, The innovation of biomaterials: from bioactive to bioelectroactive, Sci. China Mater. (2022), https://doi.org/10.1007/s40843-022-2012-3.
[16] D.-y.D. Lee, A. Prindle, J. Liu, G.M. Süel, SnapShot: electrochemical communication in biofilms, Cell 170 (1) (2017) 214, 214.
[17] A. Prindle, J. Liu, M. Asally, S. Ly, J. Garcia-Ojalvo, G.M. Süel, Ion channels enable electrical communication in bacterial communities, Nature 527 (7576) (2015) 59–63.
[18] V. Sharma, S. Chowdhury, S. Bose, B. Basu, Polydopamine codoped $BaTiO_3$-functionalized polyvinylidene fluoride coating as a piezo-biomaterial platform for an enhanced cellular response and bioactivity, ACS Biomater. Sci. Eng. 8 (1) (2022) 170–184.
[19] J. Grodstein, M. Levin, Stability and robustness properties of bioelectric networks: a computational approach, Biophys. Rev. 2 (3) (2021), 031305.
[20] M.R. Love, S. Palee, S.C. Chattipakorn, N. Chattipakorn, Effects of electrical stimulation on cell proliferation and apoptosis, J. Cell. Physiol. 233 (3) (2018) 1860–1876.
[21] S. Sundelacruz, A.T. Moody, M. Levin, D.L. Kaplan, Membrane potential depolarization alters calcium flux and phosphate signaling during osteogenic differentiation of human mesenchymal stem cells, Bioelectricity 1 (1) (2019) 56–66.
[22] S. Liu, H. Yuan, H. Bai, P. Zhang, F. Lv, L. Liu, Z. Dai, J. Bao, S. Wang, Electrochemiluminescence for electric-driven antibacterial therapeutics, J. Am. Chem. Soc. 140 (6) (2018) 2284–2291.
[23] J. Xing, S. Qi, Z. Wang, X. Yi, Z. Zhou, J. Chen, S. Huang, G. Tan, D. Chen, P. Yu, C. Ning, Antimicrobial peptide functionalized conductive nanowire array electrode as a promising candidate for bacterial environment application, Adv. Funct. Mater. 29 (23) (2019) 1806353.
[24] R. Parameswaran, J.L. Carvalho-de-Souza, Y. Jiang, M.J. Burke, J.F. Zimmerman, K. Koehler, A.W. Phillips, J. Yi, E.J. Adams, F. Bezanilla, B. Tian, Photoelectrochemical modulation of neuronal activity with free-standing coaxial silicon nanowires, Nat. Nanotechnol. 13 (3) (2018) 260–266.
[25] X. Yao, B. Zhang, S. Cui, S. Yang, X. Tang, Fabrication of $SnSO_4$-modified TiO_2 for enhance degradation performance of methyl orange (MO) and antibacterial activity, Appl. Surf. Sci. 551 (2021) 149419.
[26] J. Jiang, K. Zhao, X. Xiao, L. Zhang, Synthesis and facet-dependent photoreactivity of BiOCl single-crystalline nanosheets, J. Am. Chem. Soc. 134 (10) (2012) 4473–4476.
[27] B. Li, L. Shao, B. Zhang, R. Wang, M. Zhu, X. Gu, Understanding size-dependent properties of BiOCl nanosheets and exploring more catalysis, J. Colloid Interface Sci. 505 (2017) 653–663.
[28] Y. Fan, T. Wang, Y. Zhang, Q. Li, Z. Wu, Z. Yin, Y. Li, J. Han, Q. Wang, J. Qiu, Z. Yang, Z. Song, Enhancing the near-infrared photocatalytic activity and upconversion luminescence of BiOCl:Yb^{3+}–Er^{3+} nanosheets with polypyrrole in situ modification, J. Mater. Chem. C 9 (42) (2021) 15251–15262.
[29] W. Liu, D. Zhong, Z. Dai, Y. Liu, J. Wang, Z. Wang, J. Pan, Synergetic utilization of photoabsorption and surface facet in crystalline/amorphous contacted BiOCl-Bi_2S_3 composite for photocatalytic degradation, J. Alloys Compd. 780 (2019) 907–916.
[30] R. Chen, F. Fan, T. Dittrich, C. Li, Imaging photogenerated charge carriers on surfaces and interfaces of photocatalysts with surface photovoltage microscopy, Chem. Soc. Rev. 47 (22) (2018) 8238–8262.
[31] Y. Zhao, Z.-X. Low, Y. Pan, Z. Zhong, G. Gao, Universal water disinfection by piezoelectret aluminium oxide-based electroporation and generation of reactive oxygen species, Nano Energy 92 (2022) 106749.
[32] D.K. Yadav, S. Kumar, E.-H. Choi, M.-H. Kim, Electric-field-induced electroporation and permeation of reactive oxygen species across a skin membrane, J. Biomol. Struct. Dyn. 39 (4) (2021) 1343–1353.
[33] Y. Xu, X. Liu, Y. Zheng, C. Li, K.W. Kwok Yeung, Z. Cui, Y. Liang, Z. Li, S. Zhu, S. Wu, Ag_3PO_4 decorated black urchin-like defective TiO_2 for rapid and long-term bacteria-killing under visible light, Bioact. Mater. 6 (6) (2021) 1575–1587.
[34] X. Huang, J. Xing, Z. Wang, J. Han, R. Wang, C. Li, C. Xiao, F. Lu, J. Zhai, Z. Zhou, Y. Li, L. Zhou, Z. Song, D. Chen, P. Yu, C. Ning, X. Jiang, 0D/1D heterojunction implant with electro-mechanobiological coupling cues promotes osteogenesis, Adv. Funct. Mater. 31 (50) (2021) 2106249.

[35] C. Li, C. Xiao, L. Zhan, Z. Zhang, J. Xing, J. Zhai, Z. Zhou, G. Tan, J. Piao, Y. Zhou, S. Qi, Z. Wang, P. Yu, C. Ning, Wireless electrical stimulation at the nanoscale interface induces tumor vascular normalization, Bioact. Mater. 18 (2022) 399–408.
[36] Q. Tang, J. Liu, L.K. Shrestha, K. Ariga, Q. Ji, Antibacterial effect of silver-incorporated flake-shell nanoparticles under dual-modality, ACS Appl. Mater. Interfaces 8 (29) (2016) 18922–18929.
[37] H. Bai, H. Yuan, C. Nie, B. Wang, F. Lv, L. Liu, S. Wang, A supramolecular antibiotic switch for antibacterial regulation, Angew. Chem. Int. Ed. 54 (45) (2015) 13208–13213.
[38] Y. Zhang, D. Li, J. Tan, Z. Chang, X. Liu, W. Ma, Y. Xu, Near-infrared regulated nanozymatic/photothermal/photodynamic triple-therapy for combating multidrug-resistant bacterial infections via oxygen-vacancy molybdenum trioxide nanodots, Small 17 (1) (2021) 2005739.